






Article

Effects of PEG-Coated Silver and Gold Nanoparticles on *Spirulina platensis* Biomass during Its Growth in a Closed System

Liliana Cepoi ^{1,2} , Inga Zinicovscaia ^{3,4,*} , Ludmila Rudi ¹ , Tatiana Chiriac ¹ , Ion Rotari ¹, Vitalii Turchenko ^{3,5}  and Svetlana Djur ¹

¹ Institute of Microbiology and Biotechnology, 2028 Chisinau, Moldova; lilianacepoi@yahoo.com (L.C.); rudiludmila@gmail.com (L.R.); chiriac_tv@yahoo.com (T.C.); ioninhopld@gmail.com (I.R.); djurlana@hotmail.com (S.D.)

² Department of Biological and Geonomical Sciences, State University “Dimitrie Cantemir”, 2028 Chisinau, Moldova

³ Joint Institute for Nuclear Research, 1419890 Dubna, Russia; turchenko@jinr.ru

⁴ Horia Hulubei National Institute for R&D in Physics and Nuclear Engineering, 077125 Bucharest, Romania

⁵ Donetsk Institute of Physics and Technology named after O.O. Galkin of the NASU, 03680 Kiev, Ukraine

* Correspondence: zinikovskaia@mail.ru; Tel.: +7-496-216-5609

Received: 21 May 2020; Accepted: 21 July 2020; Published: 23 July 2020



Abstract: Silver and gold nanoparticles are promising tools for medical and industrial applications; therefore, their ecotoxicity should be carefully examined. There are many publications that discuss their effects at high concentrations on various organisms, while the effects of low doses have not been sufficiently investigated. In this paper, the effects of low concentrations of silver (12 nm) and gold (4.7 nm) nanoparticles coated with polyethylene glycol on *Spirulina platensis* biomass growth, biochemical composition, and antioxidant activity were investigated. The spirulina cultivation medium was supplemented with nanoparticles in the concentration range of 0.025–0.5 μM . The given concentrations stimulated spirulina biomass, but the content of proteins, carbohydrates, and auxiliary pigments was insignificantly affected by the presence of nanoparticles in the cultivation medium. Gold nanoparticles at a concentration of 0.5 μM produced a pronounced effect on the lipid content. Transmission electron microscope images demonstrated that the nanoparticles penetrate inside the cells and cause ultrastructural changes. The nanoparticles were characterized using several well-known techniques. The results confirmed a negative effect of low concentrations of metal nanoparticles on spirulina. This effect could be indiscernible when studying the biomass viability, but determination of the ultrastructure of the cell and the biochemical composition of the biomass could reveal it.

Keywords: *Spirulina platensis*; silver nanoparticles; gold nanoparticles; spirulina growth; biochemical composition; cell ultrastructure

1. Introduction

Engineered nanoparticles are increasingly used in biotechnology, medicine, pharmacy, ecology, electronics, agriculture, the food industry, cosmetology, and other industries due to their advantageous properties inherent to their very small sizes; most of them have already been marketed for years [1,2]. It is estimated that the current global market for nanomaterials generates production volumes from 300,000 tons up to 1.6 million tons [2]. Metallic nanoparticles are widely exploited for different applications and among them, silver (AgNPs) and gold (AuNPs) nanoparticles are highly remarkable [3].

AgNPs have a greater marketing value than other NPs, and their presence in consumer products is more widely advertised [4]. Due to their physical, optical, chemical, and antimicrobial properties, silver nanoparticles are excellent candidates for many purposes such as cancer treatment, molecular detection and diagnosis, transportation of drugs, etc. [5–7]. Nowadays, AgNPs are used in textile engineering, electronics, optics, and medical devices, as well as in different consumer products (air sanitizer sprays, pillows, respirators, socks, wet wipes, detergents, soaps, shampoos, toothpastes, washing machines, etc.) [8–10]. Another aspect of AgNPs application relates to their activity as biosensors and regulators of metabolism in plants [11,12]. In 2009, the annual worldwide AgNPs production was 500 t, and it is expected to reach approximately 800 t by 2025 [4].

AuNPs have immense applications in the fields of medicine and biotechnology because of their nontoxicity, large surface area, and unique optical, physicochemical, and biological properties [13,14]. They have suitable properties for controlled targeted drug delivery, imaging, photothermal and photodynamic therapy, the detection of cancer cells, and cancer treatment [3,15–17]. AuNPs are also widely applied in optoelectronics, photonics, catalysis, imaging technology, space science, etc. [18]. Global AuNPs consumption is projected to reach over 20 t by 2022 [19].

The exponential production and utilization of nanoparticles raise environmental concerns owing to their potentially harmful effects on the natural environment and human health [1]. The nanoparticles can be toxic to living organisms mainly because of their small size (<100 nm), large surface-to-volume ratio and highly reactive facets [20]. Since nanoparticles have the same dimensions as biological molecules, they can damage DNA, denature proteins and enzymes, and produce free radicals [5]. In humans and animals, nanoparticles easily penetrate the circulatory system, accumulate in different organs, and even translocate the blood–brain barrier [8,21].

Microorganisms, including cyanobacteria, are the primary targets exposed to nanoparticles in the natural ecosystem. Cyanobacteria have several important functions in the aquatic and terrestrial ecosystems, including CO₂ and N₂ fixation, oxygen evolution, and biomass production. They are regarded as primary producers of organic compounds [22]. Cyanobacteria have gained much attention as a rich source of bioactive compounds and have been considered one of the most promising groups of organisms to produce them [23].

As a biological test organism, the cyanobacteria *Spirulina platensis* was used. *Spirulina* contains a unique physiologically balanced combination of substances essential for the human organism: 60%–70% protein, 10%–20% carbohydrates, 5% fat, 0.9% chlorophyll, as well as vitamins, minerals, carotenoids, etc. (about 50 positions in total), and it is one of the few sources of dietary γ -linolenic acid (GLA) [24,25]. The effects of metal nanoparticles on cyanobacteria have been described in several papers [22,26–28]. However, most studies on nanoparticle toxicity investigated the effect of high concentrations of metal nanoparticles on living organisms.

The objective of the present study was to evaluate the effect of PEG-coated AgNPs and AuNPs at low concentrations (0.025–0.5 μ M) on the growth, biochemical composition, and antioxidant activity of *Spirulina platensis* biomass during its cultivation in a closed system. The changes in cell ultrastructure under the effect of the nanoparticles were assessed using transmission electron microscopy (TEM). This work contributes to a better understanding of the potential toxic effects of metal nanoparticles on aquatic organisms, in particular for the cyanobacteria *Spirulina platensis*.

2. Materials and Methods

2.1. Nanoparticles

Polyethylene glycol coated silver (PEG-AgNPs) and gold (PEG-AuNPs) nanoparticles used in this study were purchased from the M9 Company (Tolyatti, Russia). Polyethylene glycol (PEG) is a polymer that is widely used to improve the stability of metal nanoparticles in medicine manufacturing and other industries.

2.2. Nanoparticles Characterization

The zeta potential of nanoparticles was determined by photon correlation spectroscopy (PCS) using the Zetasizer Nano ZS system (Malvern Instruments, Malvern, UK). The phase composition and the type of crystal structure of the nanoparticles were analyzed by the PANalytical EMPYREAN X-ray diffractometer (EMPYREAN, Dubna, Russia) in Cu-K α radiation $\lambda = 1.541874 \text{ \AA}$. The powder diffraction software (4.8.025518) package HighScore Plus [The HighScore suite], which includes standards by the International Centre for Diffraction Data (ICDD) (<http://www.icdd.com/>), was used to identify and to refine crystal structures with Rietveld analysis (Rietveld, 1969).

2.3. Object of Study

As the object of study, the *Spirulina platensis* CNMN CB-02 strain from the National Collection of Nonpathogenic Microorganisms of the Institute of Microbiology and Biotechnology (Chisinau, Moldova) was used.

2.4. Experiment

Spirulina platensis Nordst (Geitl) CNMN-CB-02 biomass was grown in a cultivation medium with the following composition: macroelements (g/L)—NaNO₃-2.5; NaHCO₃-8.0; NaCl-1.0; K₂SO₄-1.0; Na₂HPO₄-0.2; MgSO₄·7H₂O-0.2; and microelements (mg/mL medium)—H₃BO₃-2.86; MnCl₂·4H₂O-1.81; CuSO₄·5H₂O-0.08; MoO₃-0.015; FeEDTA-1 mL/L. The spirulina was cultivated in Erlenmeyer flasks of 500 mL volume with a culture volume of 250 mL for six days, fulfilling the optimal conditions for biomass growth: temperature $30 \pm 1 \text{ }^\circ\text{C}$, pH 8–10, and illumination 37–55 μM photons/m²·s.

AgNPs and AuNPs were supplemented to the cultivation medium in a concentration range from 0.025 to 0.5 μM on the first day of biomass cultivation. In the stationary growth phase (6th day), the cyanobacteria biomass was separated from the culture medium by filtration and used for further analyses.

The quantitative parameters evaluated after the experiments were biomass quantity and the content of proteins, phycobilins, carbohydrates, β -carotene, chlorophyll a, lipids, and malondialdehyde (MDA). The obtained values for biomass were expressed in g/L, and the other parameters were expressed in percentages of dry biomass. As control, spirulina growing in a standard culture medium without the addition of nanoparticles was used.

2.5. Biochemical Analysis

Biomass quantity was determined indirectly at the end of the experiment by measuring the absorbance of the spirulina suspension at 620 nm [29,30]. The amount of biomass, expressed in g/L, was calculated based on the correlation between the absorbance of the biomass suspension and the mass of the cell fraction in the suspension. The suspension of spirulina was diluted to obtain absorbance in the range of 0.1–0.4. In this interval, the dependence of the quantity of living biomass on the absorbance is linear (Figure 1).

The protein content was determined by the Lowry method based on the formation of a copper–protein complex in alkaline conditions. For protein extraction, 10 mg of biomass was mixed with 0.9 mL of 0.1 N NaOH for 30 min. Then, 0.2 mL of the obtained hydrolysate were mixed with 0.8 mL of distilled water and 1.5 mL of a mixture of 49 parts of 2% Na₂CO₃ solution in 0.1 N NaOH and 1 part of 0.5% CuSO₄ solution in 1% C₄H₄O₆Na₂. After 10 min of reaction at room temperature, 0.5 mL of Cioaltea reagent in a dilution of 1:3 was added. The mixture was stirred for 40 min, after which the absorbance at 720 nm was measured. The protein content was determined using a calibration curve for bovine serum albumin. The test sensitivity was 2 $\mu\text{g/mL}$.

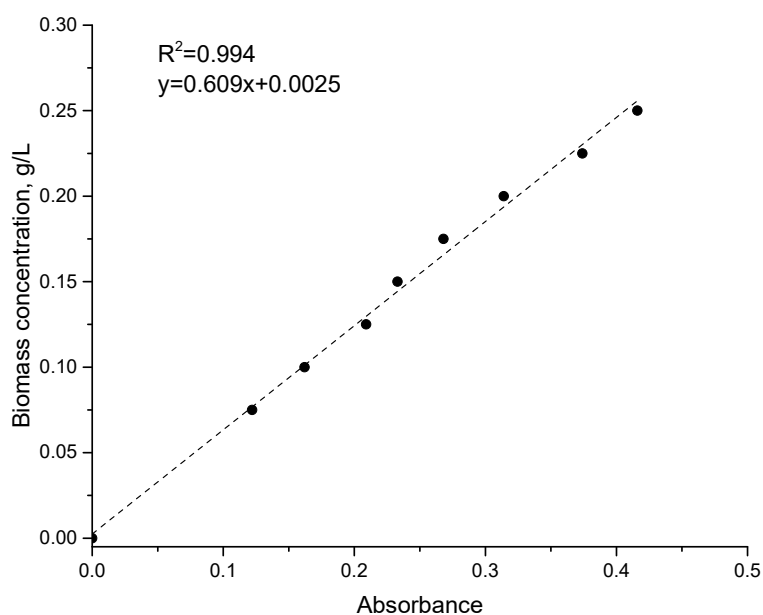


Figure 1. Correlation between the absorbance at 620 nm of a living biomass suspension of spirulina and the mass of the cell fraction.

The phycobiliprotein content was determined spectrophotometrically in water extract (10 mg/mL). The absorbance of the supernatant separated from the cells suspension by centrifugation was measured at 620 nm for c-phycoyanin and 650 nm for alo-phycoyanin. The quantity of pigments was determined based on the molar extinction coefficient: $1.54 \times 10^6 \text{ M}^{-1} \cdot \text{cm}^{-1}$ for c-phycoyanin and $0.7 \times 10^6 \text{ M}^{-1} \cdot \text{cm}^{-1}$ for alo-phycoyanin [31].

The carbohydrate content was determined by a spectrophotometric method based on the interaction of carbohydrates with the Anthon reagent ($\text{C}_{14}\text{H}_{10}\text{O}$) in acid medium. The intensity of the color of formed hydroxymethylfurfural is directly proportional to the content of carbohydrates within the limits of 0.02–0.10 $\mu\text{g/mL}$. During the experiment, 20 μL of biomass suspension (10 mg/mL) was mixed with 2 mL of 0.5% Anthon reagent in sulfuric acid (66%). Hydrolysis was carried out in a water bath for 10 min. The obtained hydrolysate was cooled and incubated at room temperature for 30 min, after which the absorbance was measured at 620 nm. The carbohydrate content was calculated using a calibration curve for glucose.

The lipid content was determined spectrophotometrically on the basis of lipid degradation using phosphovanilic reagent. For phosphovanilic reagent preparation, 0.75 g of vanillin was dissolved in 125 mL of distilled water and mixed with 500 mL of 85% o-phosphoric acid. To 10 mg of biomass, 1.0 mL of a mixture of chloroform and ethanol in a ratio of 9:1 (*v:v*) was added. Lipid extraction occurred at room temperature by shaking for 2 h. The extract was separated from the mixture and dried. The obtained precipitate was subjected to acid hydrolysis in 1 mL of sulfuric acid for 10 min, after which the samples were cooled. The obtained hydrolysate (0.1 mL) was mixed with 2.9 mL of phosphovanilic reagent. After 30 min, the absorbance was measured at 520 nm. Calculation of the lipid content was performed according to the calibration curve based on oleic acid [32].

To determine the content of chlorophyll a and β -carotene, 10 mg of spirulina biomass was mixed with 1 mL of 96% ethanol. Pigment extraction lasted 12 h by shaking the mixture at room temperature. The ethanolic extract was separated from the biomass by centrifugation. The absorbance of chlorophyll a was determined at 665 nm with an extinction coefficient $0.8 \times 10^5 \text{ M}^{-1} \cdot \text{cm}^{-1}$, and of that β -carotene was determined at 450 nm with an extinction coefficient $1.5 \times 10^5 \text{ M}^{-1} \cdot \text{cm}^{-1}$.

The content of the aforementioned biomolecules was expressed in percentage of absolute dry biomass.

Malondialdehyde (MDA) content was determined spectrophotometrically based on the reactive products of thiobarbituric acid (TBA). To 1 mL of biomass suspension (10 mg/mL), 3 mL of 0.67% thiobarbituric acid in 20% trichloroacetic acid were added. Then, the mixture was incubated for 20 min in a water bath at 100 °C. Next, the mixture was cooled and centrifuged for 15 min at 3000 g. The concentration of the malondialdehyde was measured at 535 nm (the maximum absorbance for the MDA–TBA complex) and 600 nm (for the correction of nonspecific pigmentation). The calculation was performed using the molar extinction coefficient for the malonic dialdehyde complex, 1.56×10^5 $\mu\text{M/L}$.

2.6. Antioxidant Activity by the ABTS+ Radical Cation Assay (ABTS Method)

For antioxidant tests, water extracts were prepared. For this purpose, 100.0 mg of the biomass was mixed with 10.0 mL of water and subjected to repeated freezing–unfreezing for 5 cycles. After centrifugation, the extracts were kept at 0 °C.

The total antioxidant activity of water extracts was measured by the ABTS+ (2,2-azino-bis(3-ethylbenzothiazoline-6-sulfonic acid) radical cation decolorization assay. ABTS was dissolved in distilled water to a 7 mM concentration. ABTS radical cation was produced by reacting ABTS stock solution with 2.45 mM potassium persulfate (final concentration) and allowing the mixture to stand in the dark at room temperature for 12–16 h before use. The ABTS+ stock solution was diluted with water to an absorbance of 0.7 ± 0.02 at 734 nm. Then, 1 mL of diluted ABTS+ solution was mixed with 10 μL of the test sample. After 6 min, the absorbance was measured at 734 nm.

All measurements were performed in triplicate, and the average values and standard deviation were used.

2.7. TEM Analysis

The morphology of spirulina cells before (control) and after exposure to nanoparticles (experiment) was characterized by transmission electron microscopy (TEM) using a JEM–1400 microscope (Jeol, Japan) at accelerating voltage of 100 kV. For TEM analysis, samples were fixed using 1% glutaric dialdehyde in the corresponding buffer at 4 °C for 12 h, and then by 1% OsO₄ for 1 h. Further, the samples were dehydrated using ethanol (concentration 30%–96%) and then by acetone. Fixed samples were embedded in Epon resin. Serial ultrathin sections were obtained on the ultramicrotome LKB III (LKB, Stockholm, Sweden).

3. Results

3.1. Nanoparticles Characterization

The zeta potential values determined for the analyzed nanoparticles constituted 12.1 mV for PEG–AgNPs and 27.2 mV for PEG–AuNPs, thus indicating the high stability of the colloidal system. The X-ray diffraction method (XRD) was used to examine the PEG–AgNPs and PEG–AuNPs, and the obtained XRD patterns are shown in Figure 2.

In the diffractogram obtained for AgNPs, silver crystals of cubic (Ag XRD Ref. 98–042–6921) [33] and hexagonal (Ag XRD Ref. 01–071–5025) [34] forms were present. The characteristic peaks (111) and (002) corresponded to the cubic form, while peak (101) corresponded to the hexagonal form. The wide peak in the area of 70°–90° can be attributed to an overlapping of the characteristic peaks of cubic and hexagonal forms. In case of the PEG–AuNPs, the peaks at 38.08°, 44.26°, 64.38°, 77.31°, and 81.45° can be attributed to the (111), (002), (022), (113), and (222) crystalline structures of the face-centered cubic gold (Au XRD Ref. 98–005–3763).

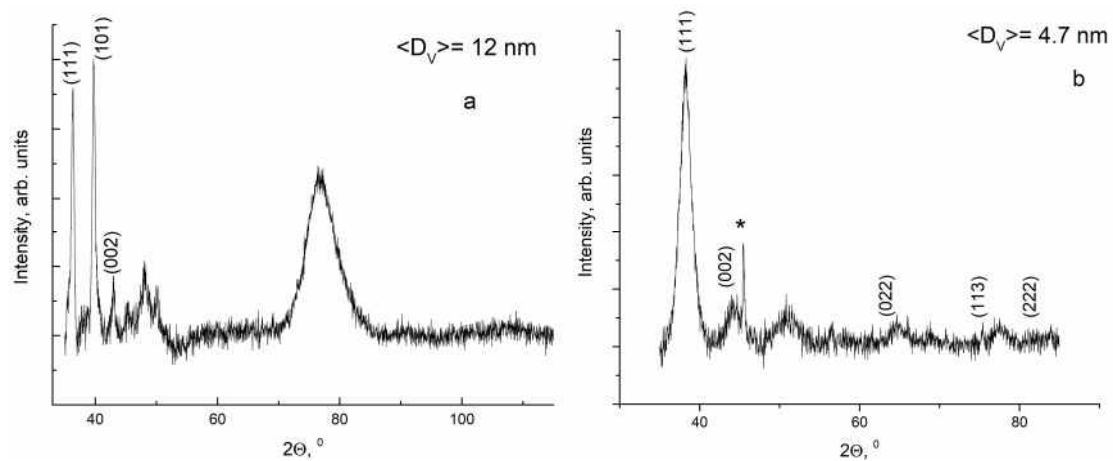


Figure 2. X-ray diffraction patterns of (a) silver nanoparticles (AgNPs) and (b) gold nanoparticles (AuNPs) measured at room temperature and fitted by the Rietveld method.

The Scherrer equation was used to determine the average size of crystallites.

$$\langle D \rangle = K\lambda / \beta \cos \theta \quad (1)$$

where K is the shape factor, which is approximately 0.9 for cubic crystals; λ is the X-ray wavelength for Cu-K α ; β is the line broadening at half the maximum intensity in radians; θ is the Bragg angle, and D is the size of a nanoparticle in \AA .

According to the calculated data, the average size of the AuNPs was approximately $4.7 \pm 0.2\text{ nm}$, while that of the AgNPs approximately $12 \pm 0.6\text{ nm}$. Since both types of nanoparticles were PEG-coated, in the further discussion, the terms AgNPs and AuNPs are used.

3.2. Effect of Silver Nanoparticles on *Spirulina platensis* Growth

The introduction of AgNPs to the cultivation medium at a concentration range of $0.025\text{--}0.1\ \mu\text{M}$ produced favorable effects on spirulina biomass, resulting in its increase by $24.2\%\text{--}31.6\%$ in comparison with the control (Figure 3). At AgNP concentrations of 0.25 and $0.5\ \mu\text{M}$, the biomass increased by 18.9% and 14.7% , respectively.

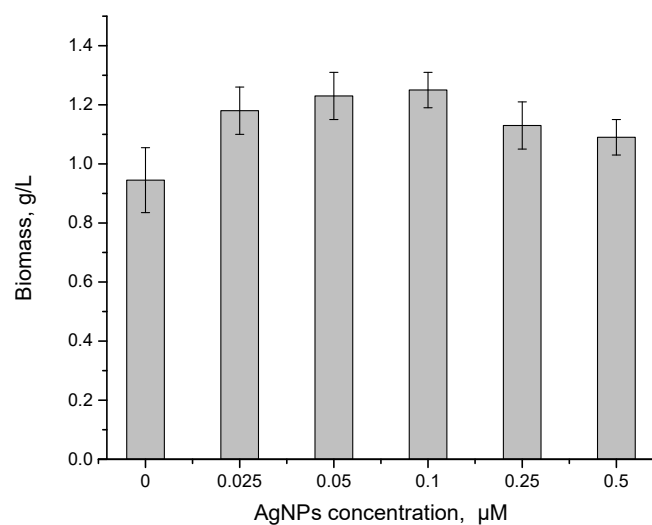


Figure 3. *Spirulina platensis* biomass at introduction of AgNPs in cultivation medium in concentration range $0.025\text{--}0.1\ \mu\text{M}$.

At AgNP concentrations of 0.05 and 0.1 μM in the medium, a slight increase of protein content by 7.0% and 9.5%, respectively, took place. At other concentrations, the increase of protein content was insignificant. The carbohydrate content in control biomass constituted 9.6%. The introduction of AgNPs in the cultivation medium at the given concentrations did not affect the biomass carbohydrate content, and it was determined to range between 8.64% and 9.54% (Figure 4). The amount of primary and secondary photosynthetic pigments (chlorophyll a, β -carotene, and phycobilins) did not change significantly under the action of AgNPs in the studied range of concentrations. Thus, the content of phycobilins in spirulina biomass varied from 10.9% to 13.8% and fell within the values characteristic for native spirulina biomass (Figure 4). The content of phycobilins in control biomass was 12.1%.

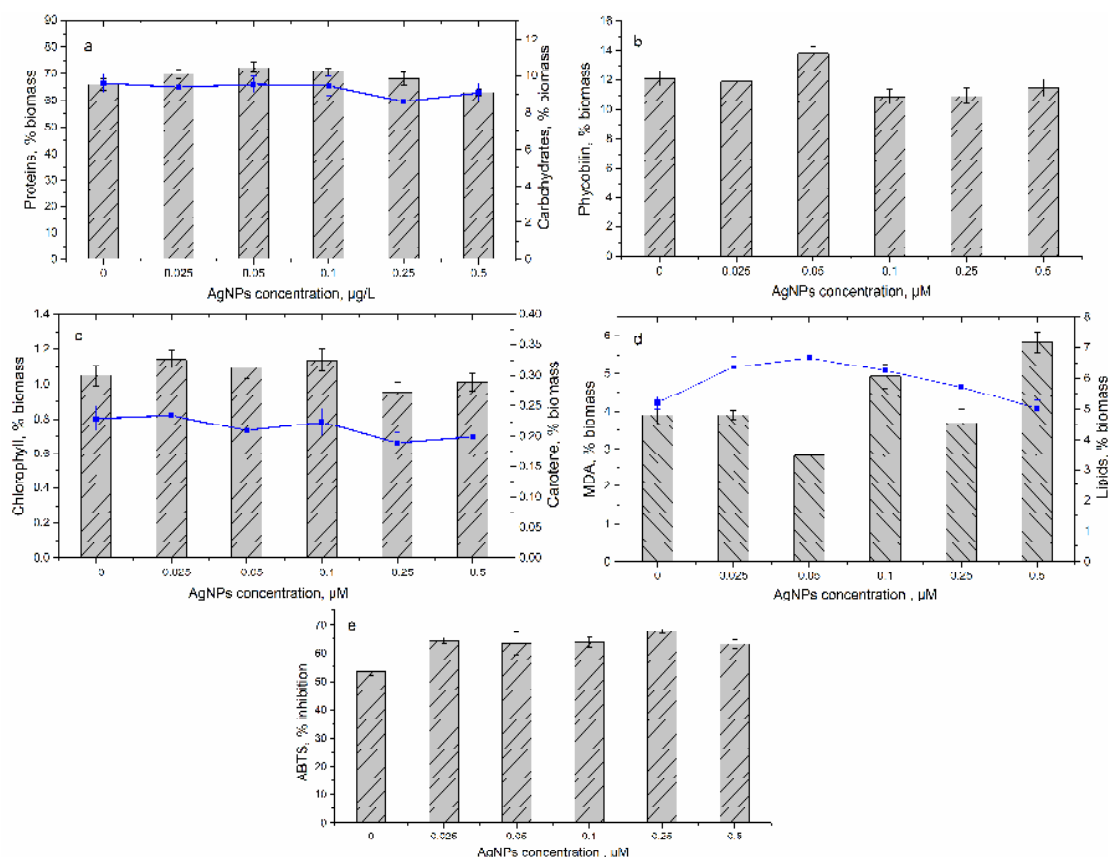


Figure 4. Change of (a) proteins and carbohydrates, (b) phycobilins, (c) β -carotene and chlorophyll a, (d) lipids and MDA content, and (e) antioxidant activity of hydric extract in *Spirulina platensis* biomass at the introduction of AgNPs in culture medium in concentration range 0.025–0.1 μM .

The contents of the two pigments (β -carotene and chlorophyll a) were very similar. The content of chlorophyll a in AgNPs-supplemented biomass varied from 0.95% to 1.14%, which was statistically insignificant. In the case of β -carotene, variations were also minor, as values ranged from 0.19% to 0.24% (Figure 4).

The components whose content changed significantly under AgNPs action were lipids. At AgNP concentration in solution of 0.025–0.1 μM , the increase in lipid content was 20.3%–28.6% in comparison with control biomass (Figure 4). The content of lipid oxidation products malondialdehyde (MDA) showed a tendency to increase at AgNP concentrations of 0.1 and 0.5 μM by 26.2% and 49.2%, respectively in comparison with control biomass.

The antioxidant activity of the water extract of spirulina biomass was also affected by the presence of NPs in the cultivation medium. Thus, at all the studied AgNP concentrations, a statistically significant increase of the antioxidant activity by 18.6%–26.7% compared to the control biomass was noticed ($p < 0.01$ for the concentrations of 0.25 and 0.5 μM and $p < 0.05$ for the other concentrations).

3.3. Effect of Gold Nanoparticles on *Spirulina platensis* Growth

The introduction of AuNPs in the cultivation medium in the concentration range 0.025–0.5 μM had a positive effect on spirulina biomass growth (Figure 5). Thus, biomass productivity increased by 29.4%–35.8% in comparison with control.

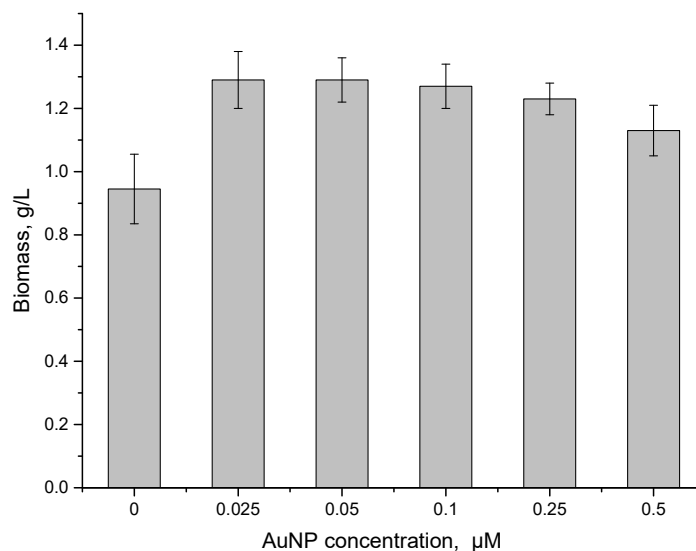


Figure 5. *Spirulina platensis* biomass at introduction of AuNPs in cultivation medium in a concentration range of 0.025–0.1 μM .

The content of proteins in biomass was not influenced by the presence of AuNPs in the cultivation medium and varied between 64.6% and 69.7% (Figure 6). The same applied to carbohydrates, whose content in biomass was not affected by AuNPs presence and was within 8.8%–9.8%. The carbohydrate content in biomass was 9.6%.

At an AuNP concentration of 0.025 μM in solution, the content of phycobilins in biomass decreased by 21%, while at a concentration of 0.1 μM , it increased by 10%. Other concentrations of AuNPs did not affect the phycobilin content, and it remained at the level of control biomass (12.1%). The content of β -carotene and chlorophyll a changed in the same way. The lowest AuNP concentration of 0.025–0.05 μM induced a decrease of the content of β -carotene by 19.8%–22.5% and of chlorophyll a by 11.3%–14.7% in comparison with native biomass (Figure 6). At a concentration range of 0.1–0.5 μM , the β -carotene content decreased by 8.4%–16.3%. AuNP concentrations of 0.1–0.5 μM did not significantly influence chlorophyll a content, and it decreased by 1%–6%.

Increases of lipid content by 33.5% and 18.7% respectively were noticed at AuNP concentrations of 0.05 and 0.10 μM . However, at an AuNP concentration of 0.5 μM , a drastic decrease of lipid content by 63.1% in comparison with native biomass took place (Figure 6). The increase of MDA content in an AuNP concentration range of 0.025–0.1 μM by 29.5%–50.8% in comparison with control biomass was noticed. An increased MDA content was also observed at an AuNP concentration of 0.5 μM by 21.3% in comparison with control biomass, which is relevant, especially taking into account the reduced content of lipids in biomass.

The antioxidant activity changed only at the lowest concentration of AuNPs in the medium, namely, 0.025 μM . At this concentration, the antioxidant activity of the water extract increased by 15.8% ($p = 0.014$), whereas at the other concentrations, it was at the level of the control biomass.

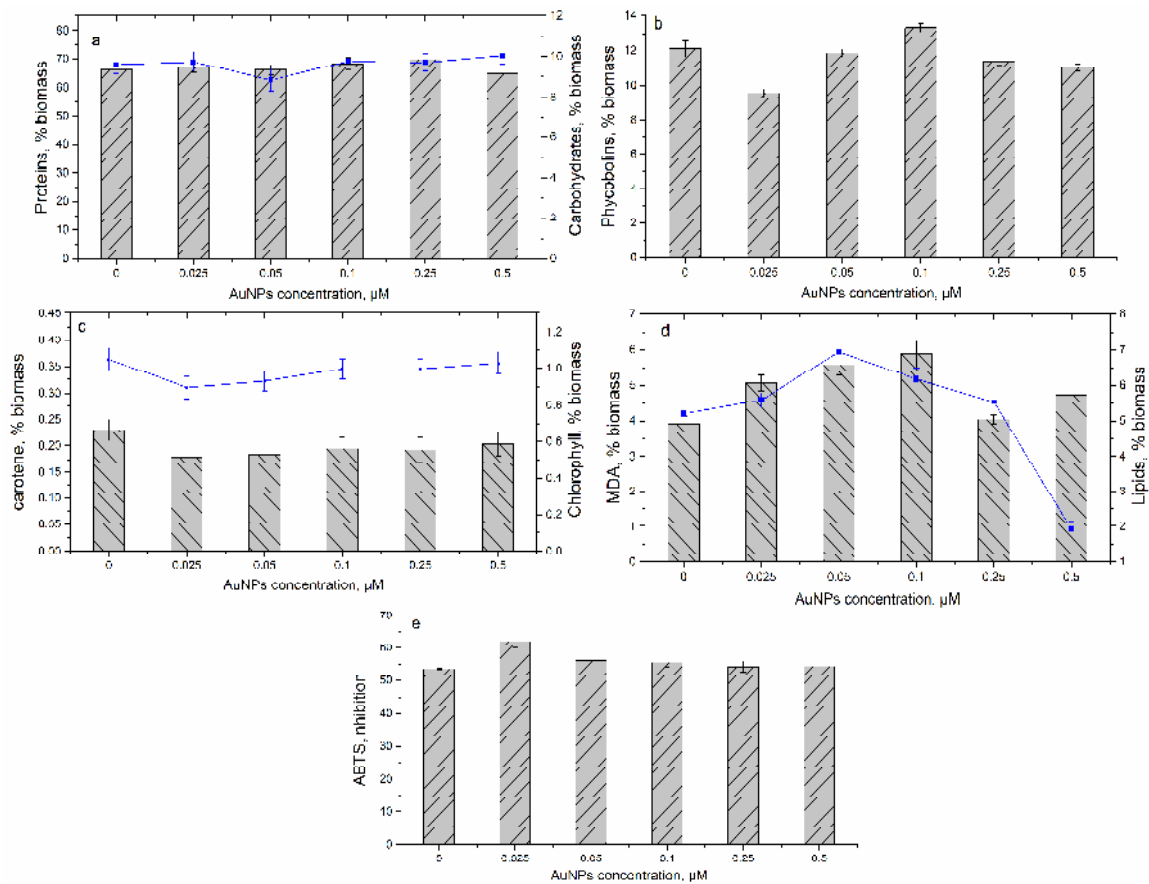


Figure 6. Change of (a) proteins and carbohydrates, (b) phycobilins, (c) β -carotene and chlorophyll *a*, (d) lipids and MDA content, and (e) antioxidant activity of hydric extract in *Spirulina platensis* biomass at the introduction of AuNPs in cultivation medium in concentration range 0.025–0.1 μM .

3.4. Transmission Electron Microscopy

As can be observed from the TEM images (Figure 7), exposure to AgNPs and AuNPs led to ultrastructural changes of the cells, depending on the concentration of nanoparticles. Micrographs of control cells showed an intact cell wall, a very thin capsule, compact thylakoids, and a large number of carboxysomes. Under the influence of nanoparticles, the cell wall became diffuse. The thylakoids in control cells are presented by a large number of dense lamellae. Nanoparticles produced a partial degradation of thylakoids. In control and AgNPs (0.05 μM)-supplemented biomass, a large number of carboxysomes—polyhedral inclusion bodies that contain the enzyme ribulose 1.5-diphosphate carboxylase/oxygenase (RuBisCO), which is responsible for carbon dioxide fixation in spirulina—was observed. In AuNPs (0.05 μM) and in AgNPs (0.5 μM)-supplemented biomass, these inclusion bodies were missing, which indicates a lower efficiency of ribulose 1.5-diphosphate carboxylase and consequently of carbon fixation. The efficiency of 1.5-diphosphate carboxylase is quite reduced, and the compartmentalization of the enzyme in carboxysome is the mechanism of carbon dioxide concentration within the scope of its fixation. The nanoparticles can be observed as an agglomeration in the cytoplasm.

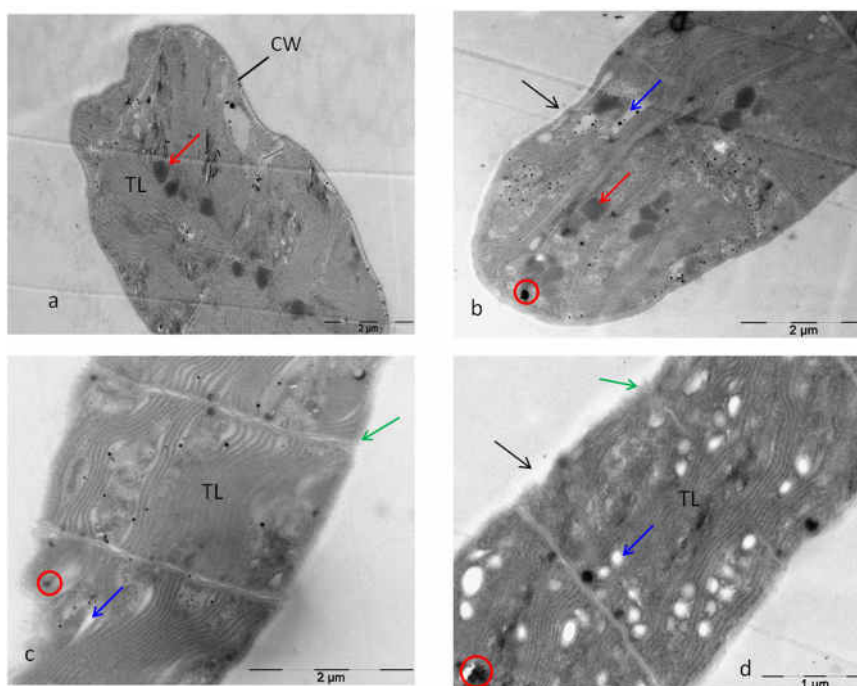


Figure 7. Transmission electron microscopy images of *Spirulina platensis* (a) control, (b) exposed to 0.05 μM AgNPs, (c) exposed to 0.05 μM AuNPs, and (d) exposed to 0.5 μM AgNPs (red arrows indicate carboxysomes; blue—vacuolated space, green—membrane rupture, TL—thylakoids, CW—cell wall, red circles—accumulated nanoparticles).

4. Discussion

The average size of the nanoparticles in the present study was determined by X-ray diffraction (XRD) and constituted 4.7 nm for AuNPs and 12 nm for AgNPs. Transmission electron microscopy and X-ray diffraction are some of the most extensively used techniques for the characterization of NPs. According to Upadhyay and co-authors [35], the particle size obtained from TEM agrees well with that obtained from XRD measurement for nanoparticles with an average size of less than 50 nm. At sizes larger than 50 nm, there are more than one crystal boundaries on the surface of the particle. It is known that XRD cannot distinguish between the two boundaries.

According to the literature data, mechanisms of metal nanoparticle toxicity can be associated with the generation of Reactive Oxygen Species (ROS), DNA damage, disturbances in the cellular phosphate management, damage on organelles, depletion of nutrients, reduction in photosynthetic yield in algae, etc. Often, AgNPs toxicity is attributed to the formation of Ag^+ ions, which easily interact with thiol groups and proteins, inactivating enzymes [4,36–38]. The toxicity of AgNPs is strongly dependent on nanoparticle size, shape, coating, and concentration. It was shown that AgNPs with sizes of less than 5 nm were more toxic to nitrifying bacteria than nanoparticles of other sizes or counterpart bulk species [36].

In the present study at an AgNP concentration range between 0.025 and 0.5 μM , cell viability and biomass biochemical composition were not affected significantly by the addition of nanoparticles to the cultivation medium. The obtained data were similar to the results of Pinzaru et al. [39], who showed a lack of toxicity of AgNPs at concentrations lower than 10 μM . The lack of toxic effect of AgNPs to cells in the present study can be explained by AgNPs coating with polyethylene glycol (PEG). Bastos et al. [40] and Pinzaru et al. [39] ascertained that PEG-coated AgNPs showed a lesser degree of toxicity to HaCat cells (Human skin keratinocytes) as compared to bare AgNPs and NPs with other types of coatings. The maintenance of a high level of productivity was also ensured by a high level of biomass antioxidant activity. At given concentrations, AgNPs did not change or produce a slight increase of the protein, carbohydrate, β -carotene, and chlorophyll a content in spirulina biomass.

In the study of Hazeem et al. [41], it was shown that AgNPs affected *Chlorella vulgaris* viability only at high AgNP concentrations (>100 mg/L). AgNPs inhibited the growth of *Chlamydomonas reinhardtii* at concentrations of 40 and 50 mg AgNPs/kg soil [42]. The highest toxicity effect on *Dunaliella salina* biomass was recorded at 1 mg/L of AgNPs at salinities (35, 70, and 140 g/L) [43].

However, some changes related to the photosynthetic machinery can be observed. One of the indicators of photosynthetic activity is the chlorophyll/carotene ratio. The value of this ratio differs from one species to another and depends on the physiological state of the photosynthetic cells. A low chlorophyll/carotene ratio is considered an indicator of stress. The values obtained in this research for the chlorophyll/carotene ratio are given in Table 1.

Table 1. Effect of nanoparticles on the chlorophyll/carotene ratio.

Type of Nanoparticles	Chl/Carotene Ratio					
	Depending on the Nanoparticles Concentration, μM					
	0 (C)	0.025	0.05	0.10	0.25	0.50
AgNPs	4.57	4.86	5.21	5.07	5.04	4.17
AuNPs	4.57	5.03	5.05	5.13	5.18	5.05

For AgNPs at concentrations of 0.025–0.25 μM , an increase of this ratio in comparison with control was observed, which indicates high photosynthesis activity. These data correlate with the increase in biomass. At an AgNP concentration of 0.50 μM , a decrease of the ratio with respect to control was noticed, which could be an indicator of a state of stress for the spirulina culture.

Carbohydrates play an important role in cell protection against different pollutants, including nanoparticles. These compounds produced by cyanobacteria can surround the cells as capsules and prevent nanoparticle penetration inside the cell [44,45]. The phycobilins are biomass components, which react promptly to pollutant impact and in a case of pronounced toxic effects, their content in biomass significantly decreases. In the performed experiments, modifications of the phycobilin content were less evident, indicating a lack of toxic effect of nanoparticles on spirulina biomass. The decrease of lipid content and the increase of MDA content at an AgNP concentration of 0.5 μM can be associated with oxidative degradation of the lipids. Thus, a possible toxic effect of AgNPs on spirulina biomass can be assumed. These data correlated with the decrease of the chlorophyll/carotene ratio. In [40], it was shown that uptake of PEG-coated AgNPs can be associated with their partial dissolution, which leads to the formation of Ag^+ ions. Thus, it can be concluded that lipids are mainly affected by PEG-coated AgNPs.

Chlorella vulgaris treated with 50 nm AgNPs showed some fluctuations in chlorophyll a concentration during a 96-h experiment, and the lowest values were recorded for cells exposed to 200 mg/L when compared to other treated samples. Cells treated with 100 nm AgNPs exhibited similar trends except for the cells treated with 10 mg/L, where the chlorophyll a concentration increased over time [41]. The effects of AgNPs (0–50 mg AgNPs/kg dry weight soil) on the soil alga *Chlamydomonas reinhardtii* after a six-day exposure were evaluated. The photosynthetic activity of *Chlamydomonas reinhardtii* in AgNP-treated soils decreased at 50 mg AgNPs/kg treated soil in comparison to the control [42].

In general, it is considered that the toxicity of AuNPs for living organisms is lower than that of AgNPs. However, as in the case of AgNPs, their toxicity is strongly dependent on factors such as the shape, size, concentration, surface charge, coating, and surface [46]. Numerous sources reported the toxicity of AuNPs to living organisms. For example, the toxicity of 4 nm polyallylamine hydrochloride-wrapped gold nanoparticles to a panel of bacteria from diverse environmental niches (*Azotobacter vinelandii*, *Acinetobacter baylyi*, *Shewanella oneidensis*, *Pseudomonas aeruginosa*) is expressed by the different minimum bactericidal concentrations determined (0.028–2.8 ppm) [47]. AuNPs were

shown to be toxic to the fungal species *Aspergillus niger*, *Mucor hiemalis*, and *Penicillium chrysogenum*, and the level of their toxicity was determined by their shape and size.

Thus, larger and non-spherical AuNPs were relatively more toxic to fungi [48]. AuNPs with a size range of 0.8–10.4 nm were tested for their antibacterial activity against pathogenic species. AuNPs with core diameters of 0.8 and 1.4 nm and a triphenylphosphine–monosulfonate shell had a minimum inhibitory concentration and minimum bactericidal concentration of 25 μM against *Staphylococcus aureus*, *Staphylococcus epidermidis*, *Escherichia coli*, and *Pseudomonas aeruginosa*. At the same time, similar-sized thiol-capped AuNPs were nontoxic even at 32-fold higher concentrations. AuNPs toxicity was associated with loss in the membrane permeability [49]. The pegylated AuNPs were found to be less toxic for the alga *Pseudokirchneriella subcapitata* compared to amphiphilic-coated particles [50]. However, according to Lehmann et al. [51], the toxicity of coated AuNPs arises from the Au core rather than from the polymer shell.

AuNPs at a concentration of 0.025–0.5 μM had a positive effect on biomass growth and did not significantly influence the protein and carbohydrate content. Sustention of the high level of productivity is also ensured by a high level of biomass antioxidant activity. At low concentrations of AuNPs, the content of β -carotene, phycobilins, and chlorophyll a in biomass decreased by more than 20%. At the same time, the chlorophyll/carotene ratio was higher compared to the control, which denotes the efficiency of the photosynthetic processes. With an increase of concentration up to 0.5 μM , the content of accessory pigments in AuNP-supplemented biomass did not change significantly. The chlorophyll/carotene ratio grew compared to the value obtained for control biomass up to the AuNP concentration of 0.25 μM , but at a concentration of 0.5 μM , there was a tendency for it to decrease, although the value was higher than in the control. These data correlated well with the increase in the amount of spirulina biomass under the influence of AuNPs.

However, at an AuNP concentration of 0.5 μM , a drastic decrease of lipid content by 63.1% in comparison with native biomass took place. The high levels of MDA in AuNP-supplemented biomass were associated with the increase of the lipid content in biomass. At an AuNP concentration of 0.5 μM , the high MDA quantity is a possible stress indicator under the conditions of minimal lipid levels. Coated AuNPs easily penetrate the hydrophobic moiety of the lipid bilayers and cause membrane disruption at increased concentration [52].

According to images obtained by TEM, both AgNPs and AuNPs caused a pronounced vacuolization of the cytoplasm, especially AgNPs at a concentration of 0.5 μM . Accumulated nanoparticles were localized mainly in the cytoplasm. The accumulation of nanoparticles leads to the release of a larger amount of extracellular polymers, which form a more pronounced layer of exopolysaccharides. As mentioned below, the external layers of polysaccharides play a protective role against toxic compounds, including nanoparticles. This finding is in agreement with Hazeem et al. [41], who reported on the storage of Ag NPs inside vacuoles in *Chlorella vulgaris*. AuNPs were capable of penetrating the thick cell wall of *Chlamydomonas reinhardtii* bacteria and formed aggregates inside the cytoplasm [53]. In a study by Pajerski et al. [54], it was shown that AuNPs of 30 nm do not penetrate the bacterial cells but adhere to the wall, which can be associated with the relatively big size of the nanoparticles.

5. Conclusions

Silver and gold nanoparticles in the concentration range of 0.025–0.5 μM stimulate the growth of spirulina biomass by 31.6% and 35.8%, respectively. Both types of NPs did not alter significantly the content of proteins, carbohydrates, and pigments. The content of lipids increased at NP concentrations of up to 0.1 μM , and their decrease at NP concentration of 0.5 μM was recorded.

The concentration of AgNPs and AuNPs of 0.5 μM entails several elements of toxicity in the spirulina culture. Among these can be mentioned the decrease of lipid content, the increase of MDA level, and the decrease of the chlorophyll/carotene ratio. Maintenance of the high level of productivity at this concentration was ensured by an adequate level the antioxidant activity of the biomass.

According to TEM images, the accumulated nanoparticles were localized mainly in the cytoplasm. The exposure to AgNPs and AuNPs resulted in ultrastructural changes of the cells expressed in membrane and cell wall ruptures, the partial degradation of thylakoids, the absence of carboxysomes, and a stronger vacuolization of the cytoplasm. At the same time, the formation of a large quantity of extracellular polymers was observed, which built a thick layer of exopolysaccharides and indicated their protective function. The obtained results show the potential hazard of the studied nanoparticles and the need to study in depth the mechanisms of nanomaterial effects on living organisms.

The potential toxicity of gold and silver nanoparticles coated with polyethylene glycol at low concentration was confirmed. It was shown that in order to identify the effects of nanoparticles, a comprehensive analysis of the viability, changes in the biochemical composition, antioxidant activity, and ultrastructure of living cells exposed to nanomaterials need to be performed.

Author Contributions: Conceptualization, L.C. and I.Z.; methodology, L.C., I.Z., L.R., and T.C.; biochemical tests performance L.R., T.C., S.D., and I.R.; XRD measurements V.T.; TEM analysis I.Z. and L.C.; validation, L.C. and L.R.; investigation, L.C.; resources, S.D.; data curation, L.R. and T.C.; writing—original draft preparation, L.C. and I.Z.; writing—review and editing, L.C. and I.Z. All authors have read and agreed to the published version of the manuscript.

Funding: This research received no external funding.

Conflicts of Interest: The authors declare no conflict of interest.

References

1. Planchon, M.; Jittawuttipoka, T.; Cassier-Chauvat, C.; Guyot, F.; Gelabert, A.; Benedetti, M.F.; Chauvat, F.; Spalla, O. Exopolysaccharides protect *Synechocystis* against the deleterious effects of titanium dioxide nanoparticles in natural and artificial waters. *J. Colloid Interface Sci.* **2013**, *405*, 35–43. [CrossRef] [PubMed]
2. Pulit-Prociak, J.; Banach, M. Silver nanoparticles—A material of the future ... ? *Open Chem.* **2016**, *14*, 76–91. [CrossRef]
3. Elahi, N.; Kamali, M.; Baghersad, M.H. Recent biomedical applications of gold nanoparticles: A review. *Talanta* **2018**, *184*, 537–556. [CrossRef] [PubMed]
4. Calderón-Jiménez, B.; Johnson, M.E.; Montoro Bustos, A.R.; Murphy, K.E.; Winchester, M.R.; Vega Baudrit, J.R. Silver nanoparticles: Technological advances, societal impacts, and metrological challenges. *Front. Chem.* **2017**, *5*, 6. [CrossRef]
5. Chaloupka, K.; Malam, Y.; Seifalian, A.M. Nanosilver as a new generation of nanoparticle in biomedical applications. *Trends Biotechnol.* **2010**, *28*, 580–588. [CrossRef]
6. Chen, H.; Gao, F.; He, R.; Cui, D. Chemiluminescence of luminol catalyzed by silver nanoparticles. *J. Colloid Interface Sci.* **2007**, *315*, 158–163. [CrossRef]
7. Nair, L.S.; Laurencin, C.T. Silver nanoparticles: Synthesis and therapeutic applications. *J. Biomed. Nanotechnol.* **2007**, *3*, 301–316. [CrossRef]
8. Prabhu, S.; Poulouse, E.K. Silver nanoparticles: Mechanism of antimicrobial action, synthesis, medical applications, and toxicity effects. *Int. Nano Lett.* **2012**, *2*, 32. [CrossRef]
9. Savithramma, N.; Linga Rao, M.; Rukmini, K.; Suvarnalatha Devi, P. Antimicrobial activity of silver nanoparticles synthesized by using medicinal plants. *Int. J. Chemtech. Res.* **2011**, *3*, 1394–1402. Available online: <https://pdfs.semanticscholar.org/a482/f5f6f29aff65a1c82f692cde97c0884ba997.pdf> (accessed on 7 June 2020).
10. Marques, L.; Martinez, G.; Guidelli, É.; Tamashiro, J.; Segato, R.; Payão, S.L.M.; Baffa, O.; Kinoshita, A. Performance on bone regeneration of a silver nanoparticle delivery system based on natural rubber membrane NRL-AgNP. *Coatings* **2020**, *10*, 323. [CrossRef]
11. Parashar, V.; Parashar, R.; Sharma, B.; Pandey, A.C. Parthenium leaf extract mediated synthesis of silver nanoparticles: A novel approach towards weed utilization. *Dig. J. Nanomater. Biostruct.* **2009**, *4*, 45–50.
12. Krishnaraj, C.; Jagan, E.G.; Ramachandran, R.; Abirami, S.M.; Mohan, N.; Kalaichelvan, P.T. Effect of biologically synthesized silver nanoparticles on *Bacopa monnieri* (Linn.) Wettst. plant growth metabolism. *Process. Biochem.* **2012**, *47*, 651–658. [CrossRef]

13. Hassanen, E.I.; Morsy, E.A.; Hussien, A.M.; Ibrahim, M.A.; Farroh, K.Y. The effect of different concentrations of gold nanoparticles on growth performance, toxicopathological and immunological parameters of broiler chickens. *Biosci. Rep.* **2020**, *40*, BSR20194296. [CrossRef]
14. Sengani, M.; Grumezescu, A.M.; Rajeswaria, V.D. Recent trends and methodologies in gold nanoparticle synthesis—A prospective review on drug delivery aspect. *Open Nano* **2017**, *2*, 37–46. [CrossRef]
15. Cabuzu, D.; Cirja, A.; Puiu, R.; Grumezescu, A.M. Biomedical applications of gold nanoparticles. *Curr. Top. Med. Chem.* **2015**, *15*, 1605–1613. [CrossRef]
16. Cai, W.; Gao, T.; Hong, H.; Sun, J. Applications of gold nanoparticles in cancer nanotechnology. *Nanotechnol. Sci. Appl.* **2008**, *1*, 17–32. [CrossRef]
17. Guo, J.; Rahme, K.; He, Y.; Li, L.L.; Holmes, J.; O'Driscoll, C. Gold nanoparticles enlighten the future of cancer theranostics. *Int. J. Nanomed.* **2017**, *12*, 6131–6152. [CrossRef]
18. Sharma, N.; Pinnaka, A.K.; Raje, M.; Fnu, A.; Bhattacharyya, M.S.; Choudhury, A.R. Exploitation of marine bacteria for production of gold nanoparticles. *Microb. Cell Factories* **2012**, *11*, 86. [CrossRef]
19. Ahuja, K.; Mamtani, K. *Gold Nanoparticles Market Size by Application (Electronics, Medical & Dentistry, Catalysis), Industry Analysis Report, Regional Outlook, Application Potential, Price Trend, Competitive Market Share & Forecast, 2015–2022*; Global Market Insights, Inc.: Selbyville, DE, USA, 2019.
20. Niazi, J.H.; Gu, M.B. Toxicity of metallic nanoparticles in microorganisms—A review. In *Atmospheric and Biological Environmental Monitoring*; Kim, Y.J., Platt, U., Gu, M.B., Iwahashi, H., Eds.; Springer: Dordrecht, The Netherlands, 2009; pp. 193–206. [CrossRef]
21. Zinicovscaia, I.; Pavlov, S.S.; Frontasyeva, M.V.; Ivlieva, A.L.; Petritskaya, E.N.; Rogatkin, D.A.; Demin, V.A. Accumulation of silver nanoparticles in mice tissues studied by neutron activation analysis. *J. Radioanal. Nucl. Chem.* **2018**, *318*, 985–989. [CrossRef]
22. Marsalek, B.; Jancula, D.; Marsalkova, E.; Mashlan, M.; Safarova, K.; Tucek, J.; Zboril, R. Multimodal action and selective toxicity of zerovalent iron nanoparticles against cyanobacteria. *Environ. Sci. Technol.* **2012**, *46*, 2316–2323. [CrossRef]
23. Abed, R.M.M.; Dobretsov, S.; Sudesh, K. Applications of cyanobacteria in biotechnology. *J. Appl. Microbiol.* **2009**, *106*, 1–12. [CrossRef] [PubMed]
24. Campanella, L.; Crescentini, G.; Avino, P. Chemical composition and nutritional evaluation of some natural and commercial food products based on Spirulina. *Analisis* **1999**, *27*, 533–540. [CrossRef]
25. Thajuddin, N.; Subramanian, G. Cyanobacterial biodiversity and potential applications in biotechnology. *Curr. Sci.* **2005**, *89*, 47–57. Available online: <https://pdfs.semanticscholar.org/98e1/4c455aa390fa156350be3b4433421785fec1.pdf> (accessed on 12 May 2020).
26. Burchardt, A.D.; Carvalho, R.N.; Valente, A.; Nativo, P.; Gilliland, D.; Garcia, C.P.; Passarella, R.; Pedroni, V.; Rossi, F.; Lettieri, T. Effects of silver nanoparticles in diatom *Thalassiosira pseudonana* and cyanobacterium *synechococcus* sp. *Environ. Sci. Technol.* **2012**, *46*, 11336–11344. [CrossRef]
27. Cherchi, C.; Gu, A.Z. Impact of titanium dioxide nanomaterials on nitrogen fixation rate and intracellular nitrogen storage in *Anabaena variabilis*. *Environ. Sci. Technol.* **2010**, *44*, 8302–8307. [CrossRef] [PubMed]
28. Shuguang, W.; Lawson, R.; Ray, P.C.; Hongtao, Y. Toxic effects of gold nanoparticles on *Salmonella typhimurium* bacteria. *Toxicol. Ind. Health* **2011**, *27*, 547–554. [CrossRef]
29. Sukumaran, P.; Nulit, R.; Zulkifly, S.; Halimoon, N.; Omar, H.; Ismail, A. Potential of fresh POME as a growth medium in mass production of *Arthrospira platensis*. *Int. J. Curr. Microbiol. Appl. Sci.* **2014**, *3*, 235–250.
30. Nor, N.M.; Naqqiuddin, M.A.; Mashor, N.; Zulkifly, S.; Oar, H.; Ismail, A. The effect of different nitrogen sources on continuous growth of *Arthrospira platensis* in simple floating photobioreactor design in outdoor conditions. *J. Algal Biomass Util.* **2015**, *6*, 1–11.
31. Boussiba, S.; Richmond, A.E. C-phycocyanin as a storage protein in the blue-green alga *Spirulina platensis*. *Arch. Microbiol.* **1980**, *123*, 143–147. [CrossRef]
32. Park, J.Y.; Jeong, H.J.; Yoon, E.Y.; Moon, S.J. Easy and rapid quantification of lipid content of marine dinoflagellates using the sulpho-phospho-vanillin method. *Algae* **2016**, *31*, 391–401. [CrossRef]
33. Lejaeghere, K.; Van Speybroeck, V.; Van Oost, G.; Cottenier, S. Error estimates for solid-state density-functional theory predictions: An overview by means of the ground-state elemental crystals. *Crit. Rev. Solid State Mater. Sci.* **2014**, *39*, 1–24. [CrossRef]
34. Novgorodovo, M.I.; Gorshkov, A.I.; Mokhov, A.V. Native silver and its new structural modifications. *Int. Geol. Rev.* **1981**, *23*, 485–494. [CrossRef]

35. Upadhyaya, S.; Parekh, K.; Pandey, B. Influence of crystallite size on the magnetic properties of Fe₃O₄ nanoparticles. *J. Alloy. Compd.* **2016**, *678*, 478–485. [[CrossRef](#)]
36. Choi, O.; Hu, Z. Size dependent and reactive oxygen species related nanosilver toxicity to nitrifying bacteria. *Environ. Sci. Technol.* **2008**, *42*, 4583–4588. [[CrossRef](#)] [[PubMed](#)]
37. Moreno-Garrido, I.; Pérez, S.; Blasco, J. Toxicity of silver and gold nanoparticles on marine microalgae. *Mar. Environ. Res.* **2015**, *111*, 60–73. [[CrossRef](#)]
38. Yang, X.; Gondikas, A.P.; Marinakos, S.M.; Auffan, M.; Liu, J.; Hsu-Kim, H.; Meyer, J.N. Mechanism of silver nanoparticle toxicity is dependent on dissolved silver and surface coating in caenorhabditis elegans. *Environ. Sci. Technol.* **2012**, *46*, 1119–1127. [[CrossRef](#)]
39. Pinzaru, I.; Coricovac, D.; Dehelean, C.; Moacă, E.A.; Mioc, M.; Baderca, F.; Sizemore, I.; Brittle, S.; Marti, D.; Calina, C.D.; et al. Stable PEG-coated silver nanoparticles—A comprehensive toxicological profile. *Food Chem. Toxicol.* **2018**, *111*, 546–556. [[CrossRef](#)]
40. Bastos, V.; Ferreira de Oliveira, J.M.P.; Brown, D.; Jonhston, H.; Malheiro, E.; Daniel-da-Silva, A.L.; Duarte, I.F.; Santos, C.; Oliveira, H. The influence of Citrate or PEG coating on silver nanoparticle toxicity to a human keratinocyte cell line. *Toxicol. Lett.* **2016**, *249*, 29–41. [[CrossRef](#)]
41. Hazeem, L.J.; Kuku, G.; Dewailly, E.; Slomianny, C.; Barras, A.; Hamdi, A.; Boukherroub, R.; Culha, M.; Bououdina, M. Toxicity effect of silver nanoparticles on photosynthetic pigment content, growth, ROS production and ultrastructural changes of microalgae *Chlorella vulgaris*. *Nanomaterials (Basel)* **2019**, *9*, 914. [[CrossRef](#)]
42. Nam, S.H.; Kwak, J.I.; An, Y.J. Quantification of silver nanoparticle toxicity to algae in soil via photosynthetic and flow-cytometric analyses. *Sci. Rep.* **2018**, *8*, 292. [[CrossRef](#)]
43. Johari, S.A.; Sarkheil, M.; Tayemeh, M.B.; Veisi, S. Influence of salinity on the toxicity of silver nanoparticles (AgNPs) and silver nitrate (AgNO₃) in halophilic microalgae, *Dunaliella salina*. *Chemosphere* **2018**, *209*, 156–162. [[CrossRef](#)]
44. Pascual García, C.; Burchardt, A.D.; Carvalho, R.N.; Gilliland, D.; António, D.C.; Rossi, F.; Lettieri, T. Detection of silver nanoparticles inside marine diatom *Thalassiosira pseudonana* by electron microscopy and focused ion beam. *PLoS ONE* **2014**, *9*, e96078. [[CrossRef](#)]
45. Pletikapić, G.; Žutić, V.; Vinković Vrček, I.; Svetličić, V. Atomic force microscopy characterization of silver nanoparticles interactions with marine diatom cells and extracellular polymeric substance. *J. Mol. Recognit.* **2012**, *25*, 309–317. [[CrossRef](#)]
46. Fratoddi, I.; Venditti, I.; Cametti, C.; Russo, M.V. How toxic are gold nanoparticles? The state-of-the-art. *Nano Res.* **2015**, *8*, 1771–1799. [[CrossRef](#)]
47. Buchman, J.T.; Rahnamoun, A.; Landy, K.M.; Zhang, X.; Vartanian, A.M.; Jacob, L.M.; Murphy, C.J.; Hernandez, R.; Haynes, C.L. Using an environmentally-relevant panel of Gram-negative bacteria to assess the toxicity of polyallylamine hydrochloride-wrapped gold nanoparticles. *Environ. Sci. Nano* **2018**, *5*, 279–288. [[CrossRef](#)]
48. Liu, K.; He, Z.; Byrne, H.J.; Curtin, J.F.; Tian, F. Investigating the role of gold nanoparticle shape and size in their toxicities to fungi. *Int. J. Environ. Res. Public Health* **2018**, *15*, 998. [[CrossRef](#)]
49. Boda, S.K.; Broda, J.; Schiefer, F.; Weber-Heynemann, J.; Hoss, M.; Simon, U.; Basu, B.; Jahnen-Dechent, W. Cytotoxicity of ultrasmall gold nanoparticles on planktonic and biofilm encapsulated gram-positive staphylococci. *Small* **2015**, *11*, 3183–3193. [[CrossRef](#)]
50. Van Hoecke, K.; De Schampelaere, K.A.C.; Ali, Z.; Zhang, F.; Elsaesser, A.; Rivera-Gil, P.; Parak, W.J.; Smaghe, G.; Hivard, C.V.; Janssen, C.R. Ecotoxicity and uptake of polymer coated gold nanoparticles. *Nanotoxicology* **2013**, *7*, 37–47. [[CrossRef](#)] [[PubMed](#)]
51. Lehmann, A.D.; Parak, W.J.; Zhang, F.; Ali, Z.; Röcker, C.; Nienhaus, G.U.; Gehr, P.; Rothen-Rutishauser, B. Fluorescent-magnetic hybrid nanoparticles induce a dose-dependent increase in proinflammatory response in lung cells in vitro correlated with intracellular localization. *Small* **2010**, *6*, 753–762. [[CrossRef](#)] [[PubMed](#)]
52. Tatur, S.; MacCarini, M.; Barker, R.; Nelson, A.; Fragneto, G. Effect of functionalized gold nanoparticles on floating lipid bilayers. *Langmuir* **2013**, *29*, 6606–6614. [[CrossRef](#)] [[PubMed](#)]

53. Mohamed, M.M.; Fouad, S.A.; Elshoky, H.A.; Mohammed, G.M.; Salaheldin, T.A. Antibacterial effect of gold nanoparticles against *Corynebacterium pseudotuberculosis*. *Int. J. Vet. Sci. Med.* **2017**, *5*, 23–29. [[CrossRef](#)] [[PubMed](#)]
54. Pajerski, W.; Ochonska, D.; Brzychczy-Wloch, M.; Indyka, P.; Jarosz, M.; Golda-Cepa, M.; Sojka, Z.; Kotarba, A. Attachment efficiency of gold nanoparticles by Gram-positive and Gram-negative bacterial strains governed by surface charges. *J. Nanoparticle Res.* **2019**, *21*, 186. [[CrossRef](#)]



© 2020 by the authors. Licensee MDPI, Basel, Switzerland. This article is an open access article distributed under the terms and conditions of the Creative Commons Attribution (CC BY) license (<http://creativecommons.org/licenses/by/4.0/>).